Received: 12 July 2023 | Revised: 21 October 2023 | Accepted: 11 December 2023

DOI: 10.1002/jnm.3205

RESEARCH ARTICLE

WILEY

Data-driven model-free modified nodal analysis circuit solver

Armin Galetzka[1] | **Dimitrios Loukrezis**[1,2] | **Herbert De Gersem**[1,2]

[1]Institute for Accelerator Science and Electromagnetic Fields, TU Darmstadt, Darmstadt, Germany

[2]Graduate School Computational Engineering, TU Darmstadt, Darmstadt, Germany

Correspondence
Herbert De Gersem, Institute for Accelerator Science and Electromagnetic Fields, TU Darmstadt, Darmstadt, Germany.
Email: degersem@temf.tu-darmstadt.de

Present address
Dimitrios Loukrezis, Schlossgartenstr. 8, Darmstadt, Germany.

Funding information
Deutsche Forschungsgemeinschaft, Grant/Award Number: GRK 2128

Abstract

This work introduces a novel data-driven model-free modified nodal analysis (MNA) circuit solver. The solver is capable of handling circuit problems featuring elements for which solely measurement data are available. Rather than utilizing hard-coded phenomenological model representations, the data-driven MNA solver reformulates the circuit problem such that the solution is found by minimizing the distance between circuit states that fulfill Kirchhoff's laws, and states belonging to the measurement data. In this way, the formerly inevitable demand for model representations is eliminated, thus avoiding the introduction of related modeling errors and uncertainties. The proposed solver is applied to linear and nonlinear RC-circuits and to a half-wave rectifier.

KEYWORDS

circuit simulation, data-driven computing, model-free solver, modified nodal analysis

1 | INTRODUCTION

Circuit simulations play a key role in the design and optimization process of electrical devices. To solve circuit problems, two types of equations are needed. On the one hand, there are Kirchhoff's laws, which describe the current and potential differences in a circuit. On the other hand, there are models that represent the actual element behavior, which are essential in classical circuit solvers. Kirchhoff's circuit laws are derived from Maxwell's equations, either in the low-frequency limit or under the assumption that the wavelength in the AC case is large compared with the circuit. Albeit these assumptions, Kirchhoff's circuit laws are derived from first principles and the equations are accepted to be exact.[1] In contrast, the models representing the lumped elements are mostly empirically known, thus introducing errors and epistemic (model-form) uncertainties arising from the modeling process.[2] Very commonly, these models are obtained via data-fitting techniques, for example, based on physically motivated approaches[3,4] or sophisticated machine learning regression methods,[5–7] to name a few options.

Nowadays, the availability of data increases steadily. For many circuit elements, the amount of behavioral data is unprecedentedly high, raising the opportunity for novel data-driven modeling, and simulation methods. Under this light, data-driven computation has emerged as and grown into a research area of its own in recent years. A model-free data-driven approach was first proposed in Ref. 8,9 for elasticity-related problems. Since then, the so-called data-driven computing framework has been extended to several other problem classes as well,[10–14] including the authors'

contributions in the field of magnetic field simulation.[15–17] The original model-free data-driven formulation[8] and its derived works are characterized by a partial differential equation (PDE), which is either elliptic or parabolic.

A common aspect in all aforementioned works is that the data-driven computing framework eliminates the previously inevitable need for model representations, for example, regarding constitutive (material) laws. Instead, a double-minimization problem is introduced to obtain the solution. Therein, the sought solution must simultaneously conform to the first-principle equations and be as close as possible to the provided measurement data. In this way, the simulation workflow is substantially reduced, as the problem at hand can be solved directly using the available measurement data, rather than investing effort in the development of model representations, which, even if considered to be adequate, remain empirical and inexact. Contrarily, using the data-driven computing framework, the modeling process and the associated errors and uncertainties are bypassed altogether.

Emerging devices commonly demand for new model representations, which are classically obtained by using physical knowledge and measurement data to determine physically inspired parameters therein. This process is very cumbersome and time-consuming, often taking several years to develop a robust physical model.[18] To address this bottleneck, this article extends data-driven computation to the case of circuit solvers, that is, the data-driven formulation is adapted to differential algebraic equations (DAEs), respectively ordinary differential equations (ODEs). In particular, a novel data-driven modified nodal analysis (MNA)[19] solver is introduced, which is able to resolve circuit problems where only data is available for certain circuit elements. Thereby, some circuit elements are assumed to be exactly known, while only measurement data is available for the remaining elements. The MNA is then reformulated along the lines of the data-driven computing framework, such that a double-minimization solver yields the states that conform to Kirchhoff's laws, while also being as close as possible to the measurements. Three numerical experiments validate the data-driven MNA method, which is able to recover reference solutions obtained with standard MNA solvers. As would be expected, the solutions of the data-driven MNA solver become increasingly more accurate as the number of available measurements increases.

The data-driven MNA solver developed in this work is substantially demarcated from other data-driven approaches found in the literature. First of all, the presented data-driven approach should not be confused with lookup table approaches,[20] which are commonly available in electronic design automation (EDA) tools. Both methods share that solely data is provided to the solver for certain elements. However, a model is generated by interpolating the data in the lookup table approach. Contrarily, the proposed data-driven approach is model-free, that is, there is no explicit or implicit modeling of the elements for which solely data is available. Other data-driven approaches[18,21,22] utilize measurement data to construct element models via machine learning (ML) techniques, instead of following the traditional modeling approach where model equations are set up using expert knowledge in semiconductor physics and subsequently calibrated based on the available measurement data. However, this approach also involves several assumptions and is essentially a regression technique. This leads to the aforementioned introduction of modeling errors and epistemic uncertainties, both of which are avoided in the proposed data-driven model-free approach.

The remaining of the article is structured as follows. In Section 2, we introduce the data-driven computing formulations in the MNA framework and derive the data-driven MNA circuit solver. Several numerical investigations are presented and discussed in Section 3, namely for a linear RC-circuit, a nonlinear RC-circuit with a voltage-dependent capacitor, and a nonlinear half-wave rectifier. A discussion on the computational cost of the data-driven MNA solver is provided in Section 4. The article is concluded with Section 5, where we summarize our findings.

2 | METHODOLOGY

2.1 | Introductory example

To showcase the idea behind the data-driven model-free circuit solver, we start with an illustrative example. We consider a circuit comprising a linear resistor, for which an exact model is available, in series with a diode, for which a set of measurement data are given. The circuit is excited by a constant voltage source v_{src}. Our goal is to find the operating point of the diode, that is, we seek for a state $(v_{\text{D}}, i) \in \mathcal{Z} \subset \mathbb{R}^2$, where v_{D} is the voltage at the diode and i the current, respectively. Employing Kirchhoff's voltage law and the model description of the resistor, we obtain as follows:

$$iR = v_{\mathrm{src}} - v_{\mathrm{D}}. \tag{1}$$

Therein, R refers to the constant and known resistor model. Thus, the solution for (v_{D}, i) is now found in the reduced space $\mathcal{K} = \{(v_{\mathrm{D}}, i) \in \mathcal{Z} : iR = v_{\mathrm{src}} - v_{\mathrm{D}}\}$. However, even the constrained set $\mathcal{K}$, which is depicted by the black line in Figure 1, contains an infinite number of solutions. Therefore, to find the operating point, information about the behavior of the diode is needed.

In a conventional solver, the information is typically given in the form of a closed-form model representation. For instance, in the case of the diode, a Shockley diode model[3] can be employed, the coefficients of which are then found by regression techniques using available measurement data. States fulfilling the model of the diode are then collected in a set $\widehat{\mathcal{D}} = \{(v_{\mathrm{D}}, i) \in \mathcal{Z} : i = f(v_{\mathrm{D}})\}$, where $f(v_{\mathrm{D}})$ represents the (nonlinear) model of the diode. The model representation of the diode is depicted by the blue line in Figure 1. Consequently, in the conventional setting, the operating point is found at the intersection of the two sets, that is, $(v_{\mathrm{D}}, i)^{\star} = \mathcal{K} \cap \widehat{\mathcal{D}}$.

In the data-driven setting, however, a model representation for the diode is not available. Instead, the measurement data are collected in a set $\mathcal{D} = \{(v_{\mathrm{D}}, i)_1, (v_{\mathrm{D}}, i)_2, ..., (v_{\mathrm{D}}, i)_N\}$, where N refers to the number of measurements. The measurement data points are shown with crosses in Figure 1. Contrarily to the conventional approach, the intersection of both sets does not necessarily yield a solution. Instead, due to finite number of measurement data points, $\mathcal{K} \cap \mathcal{D} = \emptyset$ is highly probable. Therefore, a relaxed formulation is introduced, in which we accept a solution that conforms with the circuit equations, that is, to Kirchhoff's laws, while simultaneously being closest to the available measurement data. The data-driven formulation then reads as follows:

$$(v_{\mathrm{D}}, i) = \underset{(v_{\mathrm{D}}, i) \in \mathcal{K}}{\operatorname{argmin}} \; F((v_{\mathrm{D}}, i), \mathcal{D}), \tag{2}$$

where $F((v_{\mathrm{D}}, i), \mathcal{D})$ is a distance function that returns the closest distance of a state (v_{D}, i) to the entire measurement data set. Hence, the presented data-driven framework is sometimes also referred to as a distance-minimizing data-driven computing framework. The data-driven solution for the discussed circuit is shown with a red circle in Figure 1. Note that the data-driven solution can also be found within the set of states that conform to the circuit's equation (black line in Figure 1). It is then left to the user to decide which solution, whether data-conforming or circuit-conforming, is preferred.

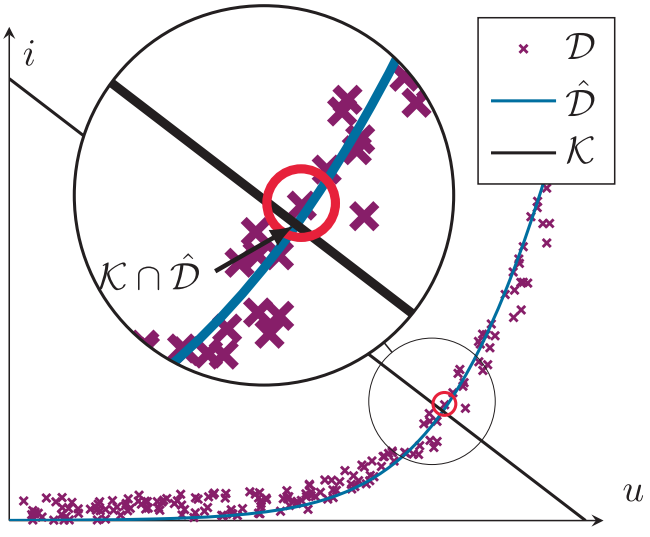

FIGURE 1 *ui* phase-space with the constraint set $\mathcal{K}$ containing all states that fulfill the circuit law (black line). The blue line represents the set $\widehat{\mathcal{D}}$ as defined by the diode model. The conventional solution is found at the intersection of both lines. The set $\mathcal{D}$ comprising the measurement data are shown by the crosses. The data-driven solution is defined by the state in the measurement data that is closest to $\mathcal{K}$ (red circle).

2.2 | Data-driven MNA solver

In this work, we consider circuits that contain passive elements, that is, resistors (G), capacitors (C) and inductors (L), voltage sources (V), and current sources (I). Let $\mathbf{A}_X \in \mathbb{R}^{(n-1)\times n_X}$ denote the reduced incidence matrices of the circuit, where n denotes the number of nodes and $X \in \{\mathrm{G},\mathrm{C},\mathrm{L},\mathrm{V},\mathrm{I}\}$. Then, employing MNA, Kirchhoff's laws are formulated as follows:

$$\mathbf{A}_\mathrm{G}\mathbf{i}_\mathrm{G}(t) + \mathbf{A}_\mathrm{C}\dot{\mathbf{q}}_\mathrm{C}(t) + \mathbf{A}_\mathrm{L}\mathbf{i}_\mathrm{L}(t) + \mathbf{A}_\mathrm{V}\mathbf{i}_\mathrm{V}(t) = -\mathbf{A}_\mathrm{I}\mathbf{i}_\mathrm{src}(t), \tag{3a}$$

$$\mathbf{A}_\mathrm{G}^\top \boldsymbol{\Phi}(t) - \mathbf{v}_\mathrm{G}(t) = 0, \tag{3b}$$

$$\mathbf{A}_\mathrm{C}^\top \boldsymbol{\Phi}(t) - \mathbf{v}_\mathrm{C}(t) = 0, \tag{3c}$$

$$\mathbf{A}_\mathrm{L}^\top \boldsymbol{\Phi}(t) - \dot{\boldsymbol{\Psi}}_\mathrm{L}(t) = 0, \tag{3d}$$

$$\mathbf{A}_\mathrm{V}^\top \boldsymbol{\Phi}(t) - \mathbf{v}_\mathrm{src}(t) = 0. \tag{3e}$$

Here, $\boldsymbol{\Phi} \in \mathbb{R}^{n-1}$ denotes the potential differences between the nodes and the mass node and $\mathbf{i}_\mathrm{G} \in \mathbb{R}^{n_\mathrm{G}}, \mathbf{i}_\mathrm{L} \in \mathbb{R}^{n_\mathrm{L}}, \mathbf{i}_\mathrm{V} \in \mathbb{R}^{n_\mathrm{V}}$, and $\mathbf{i}_\mathrm{src} \in \mathbb{R}^{n_\mathrm{src}}$ are the currents in branches with resistors, inductors, voltage sources, and current sources, respectively. The changes in charges and fluxes are denoted as $\dot{\mathbf{q}}_\mathrm{C} \in \mathbb{R}^{n_\mathrm{C}}$ and $\dot{\boldsymbol{\Psi}}_\mathrm{L} \in \mathbb{R}^{n_\mathrm{L}}$ respectively.

Applying a time-discretization scheme, for example, the backward Euler method, the time-discrete counterpart of Equation (3) reads as follows:

$$\mathbf{A}_\mathrm{G}\mathbf{i}_\mathrm{G}^{n+1} + h^{-1}\mathbf{A}_\mathrm{C}\mathbf{q}_\mathrm{C}^{n+1} + \mathbf{A}_\mathrm{L}\mathbf{i}_\mathrm{L}^{n+1} + \mathbf{A}_\mathrm{V}\mathbf{i}_\mathrm{V}^{n+1} = -\mathbf{A}_\mathrm{I}\mathbf{i}_\mathrm{src}^{n+1} + h^{-1}\mathbf{A}_\mathrm{C}\mathbf{q}_\mathrm{C}^{n}, \tag{4a}$$

$$\mathbf{A}_\mathrm{G}^\top \boldsymbol{\Phi}^{n+1} - \mathbf{v}_\mathrm{G}^{n+1} = 0, \tag{4b}$$

$$\mathbf{A}_\mathrm{C}^\top \boldsymbol{\Phi}^{n+1} - \mathbf{v}_\mathrm{C}^{n+1} = 0, \tag{4c}$$

$$\mathbf{A}_\mathrm{L}^\top \boldsymbol{\Phi}^{n+1} - h^{-1}\boldsymbol{\Psi}_\mathrm{L}^{n+1} = h^{-1}\boldsymbol{\Psi}_\mathrm{L}^{n}, \tag{4d}$$

$$\mathbf{A}_\mathrm{V}^\top \boldsymbol{\Phi}^{n+1} - \mathbf{v}_\mathrm{src}^{n+1} = 0, \tag{4e}$$

where h denotes the step size and $f^{n+1} = f(t+h)$, respectively, $f^n = f(t)$. To ease notation, we omit the superscript $^{n+1}$ in the following. We also consider the trapezoidal rule for time-discretization in our simulation. Although the derivation is straightforward, it is here omitted for brevity. In addition, it is worth mentioning that higher order backward differentiation formulas (BDFs) can be considered and numerical experiments have confirmed the expected behavior. Yet, to emphasize the novelty of the proposed approach, which is the implementation of the data-driven computing framework into the existing MNA formulation, we employ only the lowest order BDF and the trapezoidal rule.

All states that conform to Kirchhoff's laws are collected in the set $\mathcal{K} = \{\boldsymbol{\zeta} : \boldsymbol{\zeta} = (\boldsymbol{\Phi}, \mathbf{i}_\mathrm{G}, \mathbf{q}_\mathrm{C}, \boldsymbol{\Psi}, \mathbf{i}_\mathrm{L}, \mathbf{i}_\mathrm{V}) \in \mathcal{Z} : (4)\}$, where $\mathcal{Z}$ denotes the set of all possible states. For a traditional circuit solver, models for the circuit elements are needed to solve Equation (4). The models' responses can be collected in a set $\widetilde{\mathcal{D}}$, which we define as follows:

$$\widetilde{\mathcal{D}} = \left\{ \underset{e}{\times} \{i = \mathrm{G}_e(v)v\} \right\} \times \left\{ \underset{e}{\times} \{q = \mathrm{C}_e(v)v\} \right\} \times \left\{ \underset{e}{\times} \{\Psi = \mathrm{L}_e(i)i\} \right\}, \tag{5}$$

where e refers to the branch that contains the considered element. The traditional solution is again determined by $\boldsymbol{\zeta}^\star = \mathcal{K} \cap \widetilde{\mathcal{D}}$.

The need for model representations is circumvented when employing the data-driven MNA solver, within which the information on some or all circuit elements is solely available through measurement data. The per-element measurement data are collected in the sets as follows:

$$\mathcal{D}_{\mathrm{G},e} = \left\{ \left(v_{\mathrm{G}}^{\dagger}, i_{\mathrm{G}}^{\dagger} \right)_n \right\}_{n=1}^{N_{\mathrm{G},e}}, \tag{6a}$$

$$\mathcal{D}_{\mathrm{C},e} = \left\{ \left(v_{\mathrm{C}}^{\dagger}, q_{\mathrm{C}}^{\dagger} \right)_n \right\}_{n=1}^{N_{\mathrm{C},e}}, \tag{6b}$$

$$\mathcal{D}_{\mathrm{L},e} = \left\{ \left(\Psi_{\mathrm{L}}^{\dagger}, i_{\mathrm{L}}^{\dagger} \right)_n \right\}_{n=1}^{N_{\mathrm{L},e}}, \tag{6c}$$

which define the global measurement set as follows:

$$\mathcal{D} = \left\{ \underset{e}{\times} \mathcal{D}_{X,e} \right\}_{X=\{\mathrm{G,C,L}\}}, \tag{7}$$

where the cardinality of $\mathcal{D}$, that is, the total number of used measurement data points, is given by $N = \sum_e N_{\mathrm{G},e} + \sum_e N_{\mathrm{C},e} + \sum_e N_{\mathrm{L},e}$. However, searching for a solution similar to the conventional approach yields $\boldsymbol{\zeta} = \mathcal{K} \cap \mathcal{D} = \emptyset$, since only a finite number of measurement data points are available. Therefore, the data-driven framework relaxes the condition $\mathcal{K} \cap \mathcal{D}$ by accepting a solution that minimizes the distance between states that conform to Kirchhoff's laws and states belonging to the measurement set $\mathcal{D}$. We define the distance function for each element as follows:

$$f_{\mathrm{G},e}((v_{\mathrm{G}}, i_{\mathrm{G}}), \mathcal{D}_{\mathrm{G},e}) = \min_{\left(v_{\mathrm{G}}^{\dagger}, i_{\mathrm{G}}^{\dagger}\right) \in \mathcal{D}_{\mathrm{G},e}} \left\| (v_{\mathrm{G}}, i_{\mathrm{G}}) - \left(v_{\mathrm{G}}^{\dagger}, i_{\mathrm{G}}^{\dagger}\right) \right\|_{\widetilde{G}}^2, \tag{8a}$$

$$f_{\mathrm{C},e}((v_{\mathrm{C}}, q_{\mathrm{C}}), \mathcal{D}_{\mathrm{C},e}) = \min_{\left(v_{\mathrm{C}}^{\dagger}, q_{\mathrm{C}}^{\dagger}\right) \in \mathcal{D}_{\mathrm{C},e}} \left\| (v_{\mathrm{C}}, q_{\mathrm{C}}) - \left(v_{\mathrm{C}}^{\dagger}, q_{\mathrm{C}}^{\dagger}\right) \right\|_{\widetilde{C}}^2, \tag{8b}$$

$$f_{\mathrm{L},e}((\Psi_{\mathrm{L}}, i_{\mathrm{L}}), \mathcal{D}_{\mathrm{L},e}) = \min_{\left(\Psi_{\mathrm{L}}^{\dagger}, i_{\mathrm{L}}^{\dagger}\right) \in \mathcal{D}_{\mathrm{L},e}} \left\| (\Psi_{\mathrm{L}}, i_{\mathrm{L}}) - \left(\Psi_{\mathrm{L}}^{\dagger}, i_{\mathrm{L}}^{\dagger}\right) \right\|_{\widetilde{L}}^2, \tag{8c}$$

with the weighted Euclidean distance $\| (\mathbf{p}, \mathbf{q}) \|_{\widetilde{\mathbf{X}}}^2 = \sum_{i=1}^{M} \left(1/2\widetilde{X}_i^{-1} p_i^2 + 1/2\widetilde{X}_i q_i^2 \right)$, for $\mathbf{p}, \mathbf{q}, \widetilde{\mathbf{X}} \in \mathbb{R}^M$. Note that the weighting factors $\widetilde{G}, \widetilde{C}, \widetilde{L}$ are only of computational nature and do not represent the underlying element models.[8,16] For now, we only demand for constants that are bounded such that $0 < \widetilde{X} < \infty$. The global distance function is then defined as follows:

$$F(\boldsymbol{\zeta}, \mathcal{D}) = F_{\mathrm{G}}(\mathbf{v}_{\mathrm{G}}, \mathbf{i}_{\mathrm{G}}) + F_{\mathrm{C}}(\mathbf{v}_{\mathrm{C}}, \mathbf{q}_{\mathrm{C}}) + F_{\mathrm{L}}(\mathbf{i}_{\mathrm{L}}, \boldsymbol{\Psi}_{\mathrm{L}}), \tag{9}$$

where the per-element distance functions sum over all elements, that is, $F_{\mathrm{X}} = \sum_e f_{X,e}$ for $X \in \{\mathrm{G,C,L}\}$. For a given state $\boldsymbol{\zeta}$, the distance function in Equation (9) returns the minimum distance of that state to the available measurement data. To obtain a solution that fulfills Kirchhoff's laws, the minimization of Equation (9) simply needs to be constrained by Equation (4), thus resulting in the constrained minimization problem as follows:

$$\min_{\boldsymbol{\zeta}} F(\boldsymbol{\zeta}, \mathcal{D}) \tag{10}$$

subject to Equation (4), which is known as the data-driven formulation. The data-driven minimization problem in Equation (10) is essentially a double-minimization problem, which can be formulated as follows:

$$\boldsymbol{\zeta} = \arg \min_{\boldsymbol{\zeta}^{\circ} \in \mathcal{K}} \left\{ \min_{\boldsymbol{\zeta}^{\times} \in \mathcal{D}} \left\{ \| \boldsymbol{\zeta}^{\circ} - \boldsymbol{\zeta}^{\times} \|_{\widetilde{G},\widetilde{C},\widetilde{L}}^2 \right\} \right\}, \tag{11}$$

where $\| \boldsymbol{\zeta} \|_{\widetilde{G},\widetilde{C},\widetilde{L}}^2 = \| (\mathbf{v}_{\mathrm{G}}, \mathbf{i}_{\mathrm{G}}) \|_{\widetilde{G}}^2 + \| (\mathbf{v}_{\mathrm{C}}, \mathbf{q}_{\mathrm{C}}) \|_{\widetilde{C}}^2 + \| (\boldsymbol{\Psi}_{\mathrm{L}}, \mathbf{i}_{\mathrm{L}}) \|_{\widetilde{L}}^2$.

To solve Equation (11), we split the double-minimization problem into two separate minimization problems, as follows:

1. Projection on circuit state: Given a state $\boldsymbol{\zeta}^{\times} \in \mathcal{D}$, a new state $\boldsymbol{\zeta}^{\circ} \in \mathcal{K}$, which is compatible with Kirchhoff's laws and closest to a measurement state is found by solving the following term:

$$\boldsymbol{\zeta}^{\circ} = \arg\min_{\boldsymbol{\zeta} \in \mathcal{K}} \|\boldsymbol{\zeta} - \boldsymbol{\zeta}^{\times}\|^2_{\widetilde{G},\widetilde{C},\widetilde{L}}, \tag{12}$$

subject to Equation (4).

The constrained minimization problem can be solved with the help of Lagrange multipliers and by replacing the unknown voltages by potentials, which yields as follows:

$$\begin{aligned}
\mathscr{L} = &\left\|\left(\mathbf{A}_{\mathrm{G}}^{T}\boldsymbol{\Phi}, \mathbf{i}_{\mathrm{G}}\right) - \left(\mathbf{v}_{\mathrm{G}}^{\times}, \mathbf{i}_{\mathrm{G}}^{\times}\right)\right\|^2_{\widetilde{G}} + \left\|\left(\mathbf{A}_{\mathrm{C}}^{T}\boldsymbol{\Phi}, \mathbf{q}_{\mathrm{C}}\right) - \left(\mathbf{v}_{\mathrm{C}}^{\times}, \mathbf{q}_{\mathrm{C}}^{\times}\right)\right\|^2_{\widetilde{C}} + \left\|\left(\boldsymbol{\Psi}_{\mathrm{L}}, \mathbf{i}_{\mathrm{L}}\right) - \left(\boldsymbol{\Psi}_{\mathrm{L}}^{\times}, \mathbf{i}_{\mathrm{L}}^{\times}\right)\right\|^2_{\widetilde{L}} \\
&-\boldsymbol{\eta}^{\top}\left(\mathbf{A}_{\mathrm{G}}\mathbf{i}_{\mathrm{G}} + \mathbf{A}_{\mathrm{C}}\frac{\mathbf{q}_{\mathrm{C}} - \mathbf{q}_{\mathrm{C}}^{n}}{h}\right) - \boldsymbol{\eta}^{\top}\left(\mathbf{A}_{\mathrm{L}}\mathbf{i}_{\mathrm{L}} + \mathbf{A}_{\mathrm{V}}\mathbf{i}_{\mathrm{V}} + \mathbf{A}_{\mathrm{I}}\mathbf{i}_{\mathrm{src}}\right) \\
&-\boldsymbol{\lambda}_{\mathrm{L}}^{\top}\left(\mathbf{A}_{\mathrm{L}}^{T}\boldsymbol{\Phi} - \frac{\boldsymbol{\Psi}_{\mathrm{L}} - \boldsymbol{\Psi}_{\mathrm{L}}^{n}}{h}\right) - \boldsymbol{\lambda}_{\mathrm{V}}^{\top}\left(\mathbf{A}_{\mathrm{V}}^{\top}\boldsymbol{\Phi} - \mathbf{v}_{\mathrm{src}}\right).
\end{aligned} \tag{13}$$

The minimum of Equation (13) with respect to $\boldsymbol{\Phi}, \mathbf{i}_{\mathrm{G}}, \mathbf{q}_{\mathrm{C}}, \boldsymbol{\Psi}, \mathbf{i}_{\mathrm{L}}, \mathbf{i}_{\mathrm{V}}$ is found by taking the derivatives with respect to the unknowns, which results in a linear system of the form $\mathbf{M}\boldsymbol{\zeta} = \mathbf{b}$. The system matrix $\mathbf{M}$ is given by:

$$\begin{bmatrix}
\mathbf{A}_{\mathrm{G}}\widetilde{\mathbf{G}}\mathbf{A}_{\mathrm{G}}^{\top} + \mathbf{A}_{\mathrm{C}}\widetilde{\mathbf{C}}\mathbf{A}_{\mathrm{C}}^{\top} & 0 & 0 & 0 & 0 & 0 & 0 & -\mathbf{A}_{\mathrm{L}} & -\mathbf{A}_{\mathrm{V}} \\
0 & \widetilde{\mathbf{R}} & 0 & 0 & 0 & 0 & -\mathbf{A}_{\mathrm{G}}^{\top} & 0 & 0 \\
0 & 0 & \widetilde{\mathbf{K}} & 0 & 0 & 0 & -h^{-1}\mathbf{A}_{\mathrm{C}}^{\top} & 0 & 0 \\
0 & 0 & 0 & \widetilde{\mathbf{L}} & 0 & 0 & -\mathbf{A}_{\mathrm{L}}^{\top} & 0 & 0 \\
0 & 0 & 0 & 0 & \widetilde{\mathbf{M}} & 0 & 0 & h^{-1} & 0 \\
0 & 0 & 0 & 0 & 0 & 0 & -\mathbf{A}_{\mathrm{V}}^{\top} & 0 & 0 \\
0 & \mathbf{A}_{\mathrm{G}} & h^{-1}\mathbf{A}_{\mathrm{C}} & \mathbf{A}_{\mathrm{L}} & 0 & \mathbf{A}_{\mathrm{V}} & 0 & 0 & 0 \\
\mathbf{A}_{\mathrm{L}}^{\top} & 0 & 0 & 0 & -h^{-1} & 0 & 0 & 0 & 0 \\
\mathbf{A}_{\mathrm{V}}^{\top} & 0 & 0 & 0 & 0 & 0 & 0 & 0 & 0
\end{bmatrix} \quad 0 \tag{14}$$

and the right hand side reads

$$\mathbf{b} = \begin{bmatrix}
\mathbf{A}_{\mathrm{G}}\widetilde{\mathbf{G}}\mathbf{v}_{\mathrm{G}}^{\times} + \mathbf{A}_{\mathrm{C}}\widetilde{\mathbf{C}}\mathbf{v}_{\mathrm{C}}^{\times} \\
\widetilde{\mathbf{R}}\mathbf{i}_{\mathrm{G}}^{\times} \\
\widetilde{\mathbf{K}}\mathbf{q}_{\mathrm{C}}^{\times} \\
\widetilde{\mathbf{L}}\mathbf{i}_{\mathrm{L}}^{\times} \\
\widetilde{\mathbf{M}}\boldsymbol{\Psi}_{\mathrm{L}}^{\times} \\
0 \\
h^{-1}\mathbf{A}_{\mathrm{C}}\mathbf{q}_{\mathrm{C}}^{n} - \mathbf{A}_{\mathrm{I}}\mathbf{i}_{\mathrm{src}} \\
-h^{-1}\boldsymbol{\Psi}_{\mathrm{L}}^{n} \\
\mathbf{v}_{\mathrm{src}}
\end{bmatrix}. \tag{15}$$

Thus, a state $\boldsymbol{\zeta}^{\circ} \in \mathcal{K}$ that is closest to a given state $\boldsymbol{\zeta}^{\times} \in \mathcal{D}$, is obtained by

$$\boldsymbol{\zeta}^{\circ} = \mathcal{P}_{\mathcal{K}}(\boldsymbol{\zeta}^{\times}), \tag{16}$$

where $\mathcal{P}_{\mathcal{K}}$ denotes the closest point projection of a state $\boldsymbol{\zeta}^{\times} \in \mathcal{D}$ to $\mathcal{K}$.

2. Projection on measurement state: Given a state $\boldsymbol{\zeta}^\circ \in \mathcal{K}$, a new state $\boldsymbol{\zeta}^\times \in \mathcal{D}$, which belongs to the measurement set and is closest to $\boldsymbol{\zeta}^\circ$ is found by solving the following equation:

$$\boldsymbol{\zeta}^\times = \underset{\boldsymbol{\zeta} \in \mathcal{D}}{\arg\min} \|\boldsymbol{\zeta}^\circ - \boldsymbol{\zeta}\|^2_{\tilde{\tilde{G}},\tilde{\tilde{C}},\tilde{\tilde{L}}}. \tag{17}$$

Problem (17) is essentially a nearest neighbor problem, which can be solved with brute-force methods or kd-tree methods, to name but a few options.[23] Note that the minimization Problem (17) is solved independently for each element. Introducing the operator $\mathcal{P}_\mathcal{D}$ that denotes the closest point projection of a state $\boldsymbol{\zeta}^\circ \in \mathcal{K}$ to $\mathcal{D}$, a new state $\boldsymbol{\zeta}^\times \in \mathcal{D}$ is obtained through

$$\boldsymbol{\zeta}^\times = \mathcal{P}_\mathcal{D}(\boldsymbol{\zeta}^\circ). \tag{18}$$

Thus, for each solver iteration, the two minimization Problems (12) and (17) must be solved. Depending on the initial value, the iteration scheme can be defined as follows:

$$\boldsymbol{\zeta}^\circ_{p+1} = (\mathcal{P}_\mathcal{M} \circ \mathcal{P}_\mathcal{D})\left(\boldsymbol{\zeta}^\circ_p\right), \tag{19}$$

respectively,

$$\boldsymbol{\zeta}^\times_{p+1} = (\mathcal{P}_\mathcal{D} \circ \mathcal{P}_\mathcal{M})\left(\boldsymbol{\zeta}^\times_p\right), \tag{20}$$

which can be seen as a fixed-point iteration, as visually illustrated in Figure 2. This minimization procedure is carried out until either $\boldsymbol{\zeta}^\circ_p$ and $\boldsymbol{\zeta}^\times_p$ do not change after two consecutive iterations or until a desired accuracy is reached. The accuracy at iteration p can be measured in terms of the distance, equivalently, the mismatch between states conforming to Kirchhoff's laws to states found in the measurement set. This mismatch is defined as follows:

$$\varepsilon^2_{\mathrm{m},p} = \left\|\boldsymbol{\zeta}^\circ_p - \boldsymbol{\zeta}^\times_p\right\|^2_{\tilde{\tilde{G}},\tilde{\tilde{C}},\tilde{\tilde{L}}}, \tag{21}$$

which is essentially the weighted distance between the two states. Convergence is achieved when the change in the mismatch (Equation (21)) between two consecutive iterations is below a user-defined tolerance $\delta_{\varepsilon_\mathrm{m}}$. Once the data-driven solver has converged, we carry on with the next time step. The most recent data-driven solution is employed as starting point in the new time step.

Overall, the double-minimization problem is a challenging non-convex optimization problem characterized by numerous local minima. However, numerical experiments in several works[8,24] have demonstrated that the data-driven solution remains a reliable approximation of the conventional solution even when the global minimum cannot be reached. The non-convexity relaxes if adaptively adjusted weighting factors are utilized,[16,25] which increases the solution accuracy and reduces both statistical dispersion and computational time. In principle, it is possible to locate the

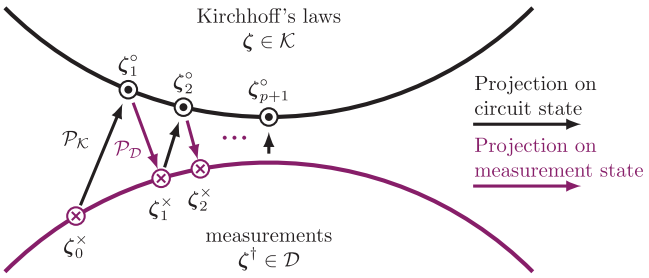

FIGURE 2 Illustration of the fixed-point iteration.

ALGORITHM 1 **Data-driven model-free MNA solver. The time axis has been discretized into K time steps.**

Randomly initialize measurement states $\boldsymbol{\zeta}^{\times} \in \mathcal{D}$
for $k = 1, \ldots, K$ **do**
  while $|\, \varepsilon_{\mathrm{m},p} - \varepsilon_{\mathrm{m},p-1} \,| > \delta_{\varepsilon_\mathrm{m}}$ **do**
    solve linear system $\mathbf{M}\boldsymbol{\zeta}_p^{\circ} = \mathbf{b}$
    find $\boldsymbol{\zeta}_p^{\times}$ in $\mathcal{D}$ adjacent to $\boldsymbol{\zeta}_p^{\circ}$ with (17)
    compute $\varepsilon_{\mathrm{m},p}$ with (21)
  end while
end for

global minimum through the application of mixed-integer programming,[26] irrespective of the chosen weighting factor. However, this method becomes computationally infeasible when handling large datasets or a high number of degrees of freedom. Finally, the original method[8] has been proven to converge toward the conventional solution under specific conditions related to the measurement set.[27] This convergence result remains consistent regardless of the chosen phase-space norm. This proof has been originally established for elliptic PDEs, however, we expect a seamless transition to our use case as it has been shown that circuits can be translated into PDEs.[28]

It is customary that most of the elements in a circuit are well-known and model representations are available. In this case, various approaches combining exactly known models with data-driven computing have been proposed by the authors in Ref. 15, in the context of magnetic field simulation. We consider the least intrusive approach, where the minimization (Equation (17)) is now performed to the known model representation. In addition, the weighting factors in Equations (14) and (15) are chosen according to the known model coefficients. Furthermore, it has been shown by the authors that, for elements featuring a strongly nonlinear response and/or data-starved or unevenly filled measurement sets, constant weighting factors hinder the convergence rate of the data-driven solver.[16] Therefore, we follow the approach developed in Ref. 16 and choose the weighting factors to be the local tangent of the current state with respect to the surrounding states in the measurement set.

The data-driven MNA solver is summarized in Algorithm 1.

3 | NUMERICAL EXPERIMENTS

In the following, we consider different circuit configurations. To validate the data-driven solver, we generate synthetic measurement data sets of increasing cardinality, for each of which the circuit is solved. At every time step $t_k, k = 1, \ldots, K$, and at a specific element $X \in \{\mathrm{G}, \mathrm{C}, \mathrm{L}\}$, we calculate the mismatch of the data-driven solution to a reference solution, for example, obtained with a traditional MNA solver utilizing the "true" circuit elements. The mismatch error is defined as follows:

$$\varepsilon^2_{\mathrm{M},\widetilde{X}}(t) = \left\| (p_{\mathrm{ref}}, q_{\mathrm{ref}}) - (p, q) \right\|^2_{\widetilde{X}} \Big|_t . \tag{22}$$

Furthermore, we define the root mean square (RMS) error over the entire time interval as follows:

$$\varepsilon_{\mathrm{RMS},\widetilde{X}} = \left(\frac{\int_{t_0}^{T} \varepsilon^2_{\mathrm{M},\widetilde{X}}(t)\,\mathrm{d}t}{\int_{t_0}^{T} \left(\left\| (p_{\mathrm{ref}}, q_{\mathrm{ref}}) \right\|^2_{\widetilde{X}} \right) \mathrm{d}t} \right)^{\frac{1}{2}} \approx \left(\frac{\sum_{k=0}^{K} \varepsilon^2_{\mathrm{M},\widetilde{X}}(t_k)}{\sum_{k=0}^{K} \left(\left\| (p_{\mathrm{ref}}, q_{\mathrm{ref}}) \right\|^2_{\widetilde{X}} \right) \Big|_{t_k}} \right)^{\frac{1}{2}} . \tag{23}$$

The weighting factors in Equations (22) and (23) correspond to the actual model parameters, which are used for the reference solution.

We note that the presented convergence results are only meaningful under the assumption that the conventional solution serves as the ground truth. However, this assumption does not hold in real-world scenarios where empirical models are constructed from actual measurement data. In such cases, it is indeed difficult to establish a meaningful error norm between the data-driven and the conventional approach, primarily because the true behavior of the elements is unknown, thus making unclear what should be considered as the definitive reference point or ground truth.[17] Furthermore, the required level of accuracy is highly dependent on the specific use case. In addition to errors stemming from finite data, there are numerous other error sources to consider, such as time-discretization, mathematical modeling of the physical problem, and general numerical approximations, to name but a few.

3.1 | Introductory example revisited

Before considering time-dependent ODE problems, we revisit the pure algebraic problem introduced in Section 2.1. The associated minimization problem reads as follows:

$$\min_{v_\mathrm{D}} \min_{\left(v_\mathrm{D}^\times, i_\mathrm{D}^\times\right) \in \widetilde{D}} F\left(v_\mathrm{D}, \widetilde{\mathcal{D}}\right) = \min_{v_\mathrm{D}} \min_{\left(v_\mathrm{D}^\times, i_\mathrm{D}^\times\right) \in \widetilde{D}} \left\{ \widetilde{R}_\mathrm{D} \left(\frac{v_\mathrm{src}}{R} - \frac{v_\mathrm{src}}{R} - i_\mathrm{D}^\times \right)^2 + \widetilde{G}_\mathrm{D} \left(v_\mathrm{D} - v_\mathrm{D}^\times \right)^2 \right\}, \tag{24}$$

where $\widetilde{R}_\mathrm{D} = 1/\widetilde{G}_\mathrm{D}$ refers to the weighting factor. In the following discussion, our focus is on analyzing the impact of the initial value in the fixed-point iteration scheme on its solution. Figure 3A illustrates the iterative process for two distinct initial starting points. We can clearly observe that two distinct solutions are obtained, depending on the starting value. However, both solutions are in close proximity to the actual solution. This is due to the adaptively adjusted weighting factor, which balances the two summation terms in Equation (24) and additionally mitigates the inherent non-convexity of Equation (24). To further illustrate this effect, Figure 3B depicts the normalized loss of the minimization problem in Equation (24) for both an adaptively adjusted weighting factor and different choices of constant weighting factors. One can clearly observe that, if a constant weighting factor is utilized, several minima occur. Depending on the initial point, the fixed-point iteration can become stuck in a local minimum. Conversely, when employing an adaptively adjusted weighting factor, the minimization problem exhibits a smoother response surface, making it easier to identify the global optimum.

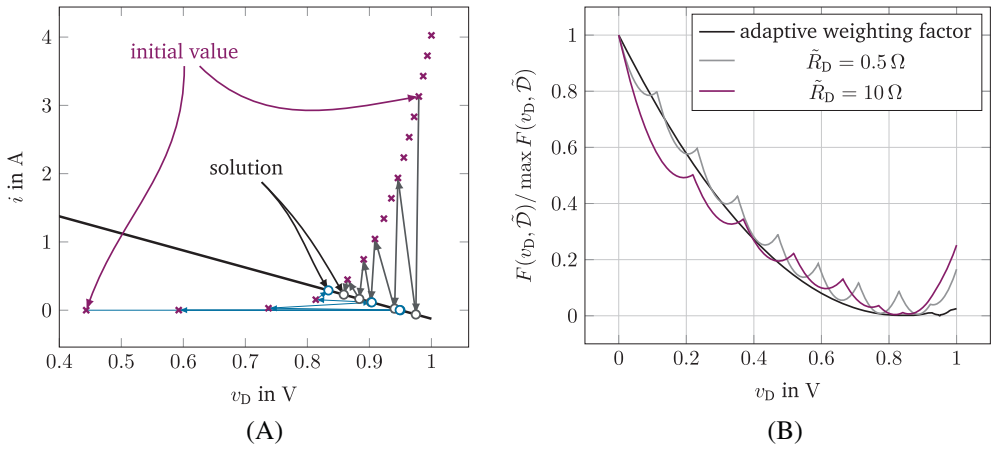

FIGURE 3 (A) Fixed-point iteration for the resistor-diode circuit. States that fulfill the circuit law are shown by the black line, whereas the measurement data points of the diode are indicated by the purple crosses. The results have been computed utilizing an adaptive weighting factor and show the iterative process for two distinct initial values. (B) Normalized loss of the minimization problem for the resistor-diode circuit. The loss is shown for different choices of the weighting factor, including an adaptive weighting factor.

3.2 | Linear RC-circuit

For a first test, we consider an RC-circuit, with resistor R and capacitor C in series. The circuit acts as an academic test case and allows us to discuss the error sources appearing within the data-driven solver. In order to use the analytical solution as a reference, we consider only linear elements. The circuit is excited by a constant voltage source, with the initial value $q_C(t=0)=0$. We employ a data-driven solver combined with the backward Euler scheme and the trapezoidal rule, where for the resistor and capacitor only measurement data are available. In addition, solutions for different step sizes h, equivalently, numbers of time steps, are computed.

Figure 4A shows the RMS error for solutions obtained with the backward Euler method and the trapezoidal rule for different numbers of time steps. Furthermore, the RMS error for a traditional MNA solver is shown. The results show that the accuracy of the data-driven solution improves as more measurement data are employed. However, for certain combinations of employed measurement data and number of time steps, the convergence stagnates. To analyze this behavior, we consider the overall error of a state (p,q) to the reference solution. The error is given as

$$\begin{aligned}\varepsilon &= \|(p_{\text{ref}},q_{\text{ref}})-(p,q)\|_{\widetilde{X}}^2,\\ &= \|(p_{\text{ref}}-p_{\text{trad}},q_{\text{ref}}-q_{\text{trad}})-(p-p_{\text{trad}},q-q_{\text{trad}})\|_{\widetilde{X}}^2,\\ &\le \underbrace{\|(p_{\text{ref}},q_{\text{ref}})-(p_{\text{trad}},q_{\text{trad}})\|_{\widetilde{X}}^2}_{\varepsilon_{\text{time}}}+\underbrace{\|(p,q)-(p_{\text{trad}},q_{\text{trad}})\|_{\widetilde{X}}^2}_{\varepsilon_{\text{data}}},\end{aligned} \tag{25}$$

where $(p_{\text{trad}},q_{\text{trad}})$ is a state computed with a traditional MNA solver. Hence, the overall error can be decomposed into an error stemming from the time-discretization scheme and an error attributed to the finite measurement data. This decomposition can be clearly observed in Figure 4A. The figure shows several cases where extending the measurement set does not lead to an improvement in the accuracy. In those cases, the time-discretization error $\varepsilon_{\text{time}}$ is dominant and the accuracy of the data-driven solver stagnates at the accuracy level of the traditional solver. Hence, to avoid unnecessary computational costs, the time-discretization scheme and the number of employed measurement data points should preferably be chosen according to one another. In cases where the time-discretization error $\varepsilon_{\text{time}}$ is negligible, for example, for $K=1000$ time steps and the trapezoidal rule, the data-driven solver achieves a linear convergence rate with respect to the employed measurement data.

Next, we focus on the error attributed to the limited measurement data. Therefore, the circuit is simulated using the trapezoidal rule and $K=1000$ time steps. The reference solution v_C as well as data-driven solutions for measurement data

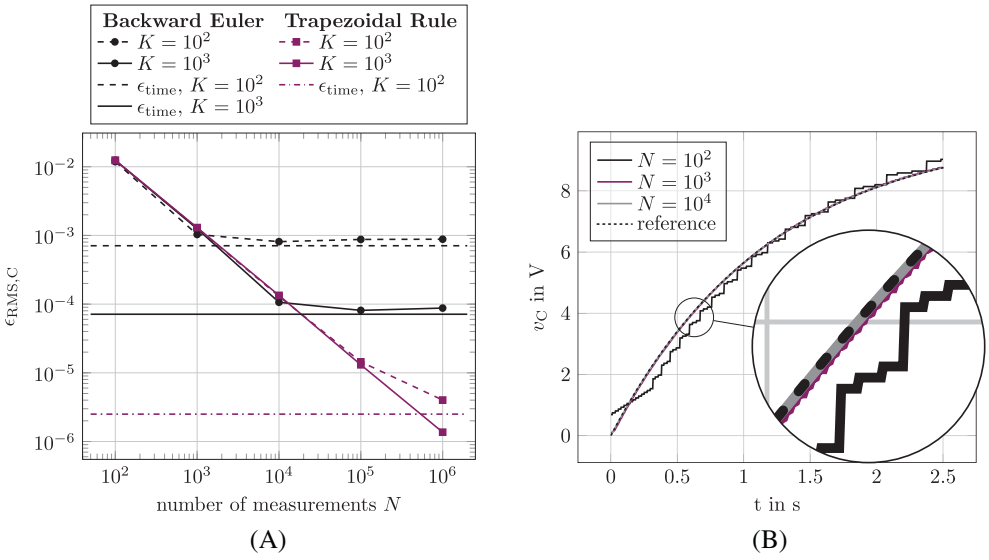

FIGURE 4 Linear RC-circuit: (A) RMS error at the capacitor C over number of measurements. The horizontal lines mark the time-discretization errors for a traditional MNA circuit solver. (B) Voltage v_C at the capacitor over time. The plot shows the analytical reference solution, as well as data-driven solutions for an increasing number of measurement data points.

sets of increasing size are depicted in Figure 4B. We can already qualitatively observe that, if the measurement data set is not sufficiently large, for example, for $N = 10^2$, the solution of the data-driven solver captures the behavior of the circuit, albeit a large error to the analytic solution remains. Furthermore, the figure shows that, due to the discrete data, the solution is not continuous and exhibits jumps at certain time steps. More precisely, due to the finite data, the solver might select the same measurement state in consecutive time steps or migrate to a new measurement state in a next time step. However, as more data becomes available, these discontinuities are reduced. Figure 5 shows the mismatch to the reference solution over time for measurement sets of increasing cardinality. The figure clearly shows that the solution accuracy increases with the number of measurement data points. Furthermore, we observe that the error varies in time, which is attributed to the change in the circuit's operating point over time by constant measurement set. That is, in certain time steps, the available measurement data suit better to the operating point than in others.

3.3 | Nonlinear RC-circuit

We revisit the RC-circuit, yet this time we consider a voltage-dependent capacitor $C(v_C(t))$. The response of the capacitor as well as the charge over the applied voltage is shown in Figure 6A. This nonlinear response is the typical behavior

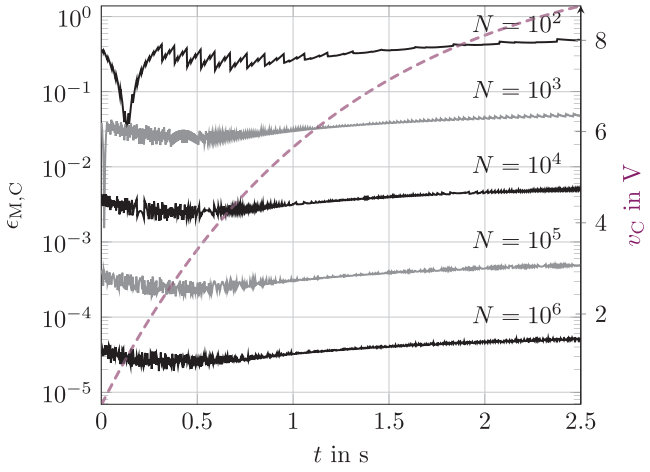

FIGURE 5 Linear RC-circuit: Error at the capacitor C over time. The error is shown for an increasing number of measurement data $N \in \{10^2, 10^3, 10^4, 10^5, 10^6\}$. The dashed line shows the voltage v_C.

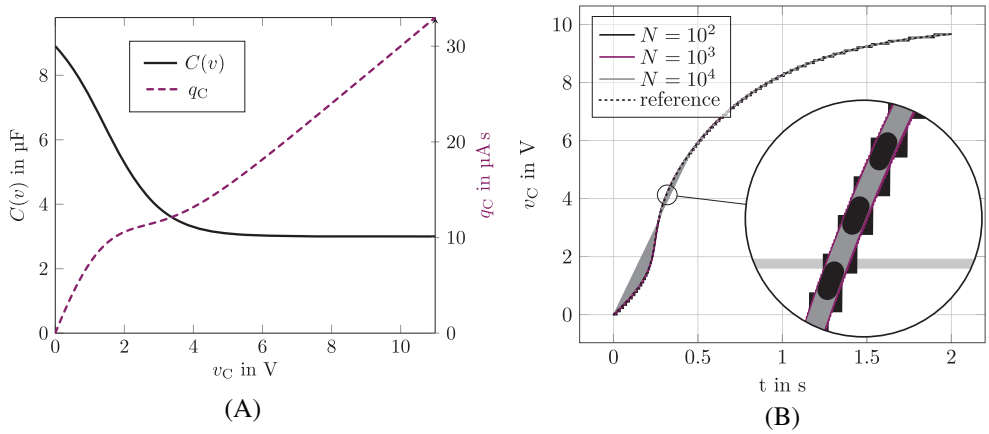

FIGURE 6 Nonlinear RC-circuit: (A) Voltage-dependent capacitor $C(v_C)$ and charge $q_C(v_C)$ over applied voltage v_C. (B) Voltage v_C at the capacitor over time. The plot shows the analytical reference solution, as well as data-driven solutions for an increasing number of measurement data $N \in \{10^2, 10^3, 10^4\}$.

of multilayer ceramic capacitors, for which the capacitance drops rapidly for moderate voltages to a nearly constant value.[29,30]

The data-driven solver treats the resistor as a known element. Contrarily, only measurement data is available for the voltage-dependent capacitor. To validate the results obtained with the data-driven solver, we generate measurement data sets of increasing cardinality. Both the reference solver and the data-driven solver employ the trapezoidal rule for time-discretization. Figure 6B shows the capacitor voltage over time. Similar to the linear case, the data-driven solution shows large jumps between the time steps if the number of measurement data points is not sufficiently large. As the number of measurements increases, the data-driven solution becomes increasingly smoother and eventually identical to the conventional MNA solution. This is also evident by the results shown in Figure 7A regarding the RMS error over time for an increasing number of measurement data points. Similar to the linear RC-circuit, a linear convergence rate with respect to the number of measurement points is observed. The mismatch over time and for measurement sets of increasing cardinality is shown in Figure 7B. Again, the figure clearly shows that the solution accuracy increases with the number of measurement data points. We also observe that the error in time is slightly larger in the strongly nonlinear region, that is, for $t < 0.5$, respectively for $v_C < 4$.

3.4 | Half-wave rectifier

The next test case considers a half-wave rectifier circuit, depicted in Figure 8A. The circuit elements are $R_C = 1$, $R_D = 10$, $C = 100$ and $v_{src} = 5\sin(\omega t)$, where $\omega = 2\pi f$ and $f = 100$. The diode is modeled using the Shockley diode model,[3] such that

$$i(t) = i_s\left(e^{\frac{v_D(t)}{n v_T}} - 1\right), \tag{26}$$

where v_D is the voltage at the diode, $i_s = 2.52$ nA is the saturation current, $v_T = 25.85$ mV is the thermal voltage, here for $T = 300$ K, and $n = 1.752$ is the ideality factor. The initial value is $q_C(t = 0) = 0$ As.

We assume that the resistors and the capacitor are known elements, whereas the diode is only known by measurement data. The parasitic resistor R_D is part of the circuit model in the NGSPICE simulation.[31] Hence, the measurement data are generated from the diode model including the parasitic resistor R_D. The data-driven solutions are compared with a reference solution obtained with NGSPICE. For both the reference and the data-driven solutions, $K = 400$ time steps are used. The data-driven solver is based on the trapezoidal rule. Figure 8B shows the output voltage v_C of the half-wave rectifier. The figure clearly shows that the data-driven solution becomes more accurate if more measurement data points are employed. However, we also observe that a rather large number of measurement data points are needed to achieve an adequately accurate solution. This behavior can also be seen in Figure 9A, which shows the mismatch over time, as well as in Figure 9B, which shows the RMS error at the capacitor. The reduced convergence rate can be

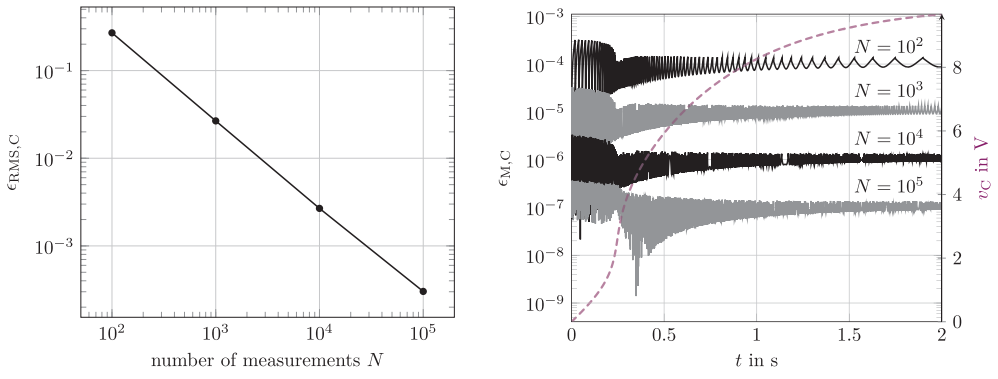

FIGURE 7 Nonlinear RC-circuit: (A) RMS error at the capacitor C over number of measurements. (B) Error at the capacitor C over time. The error is shown for an increasing number of measurement data $N \in \{10^2, 10^3, 10^4, 10^5\}$. The dashed line shows the voltage v_C.

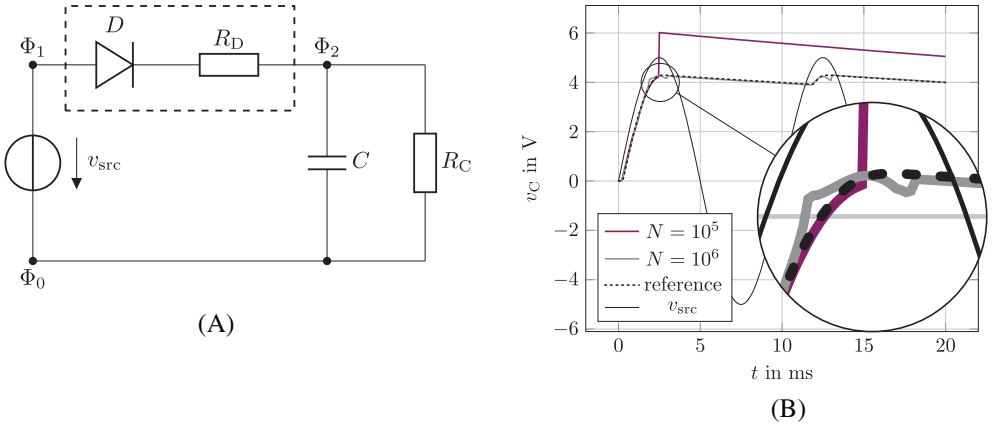

FIGURE 8 Half-wave rectifier: (A) Circuit. (B) Voltage v_C at the capacitor over time. The plot shows the reference solution obtained with NGSPICE and data-driven solutions for an increasing number of measurement data $N \in \{10^5, 10^6\}$.

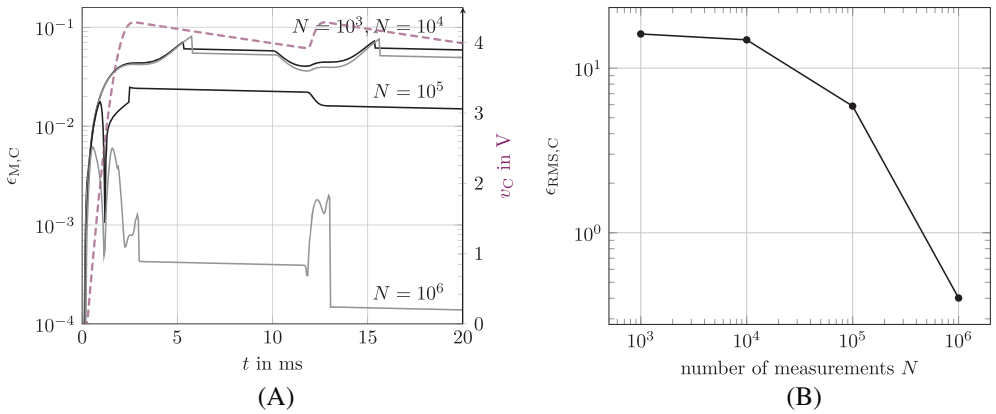

FIGURE 9 Half-wave rectifier: (A) Error at the capacitor C over time. The error is shown for an increasing number of measurement data $N \in \{10^3, 10^4, 10^5, 10^6\}$. The dashed line shows the output voltage v_C. (B) RMS error at the capacitor C over number of measurements.

explained by the switching behavior of the diode. That is, the distance-minimizing data-driven solver faces problems in the regime where the current of the diode remains almost constant, that is, for $v_D \ll v_{fv}$, where v_{fv} is the forward threshold voltage.

Although out of scope for this work, the aforementioned problem could be tackled by employing hybrid models for the diode.[32] In that case, the diode's phase-space would be partitioned into two segments: one employing a conventional model and the other utilizing solely measurements. The data-driven solver would then switch between these models based on a specified threshold. By that, the part of the phase-space where it is difficult to find a suitable model is treated using the data-driven formulation, thus mitigating the aforementioned errors. In the particular case of the diode, a linear model could be employed for $v_D \ll v_{fv}$.

4 | COMPUTATIONAL COST

In the following, we briefly discuss the computational cost of the data-driven MNA solver. A more detailed discussion on the computational complexity of data-driven solvers is available in the authors' prior works.[16,17]

In each data-driven iteration, we have to solve a linear system of size $N_M = 2n - 2 + n_G + n_C + 3n_L + 2n_V$, which amounts to $\mathcal{O}(N_M^3)$ if standard direct linear system solvers a used. Afterwards, $N_{dd-elem}$ nearest neighbor problems must be solved, where $N_{dd-elem}$ refers to the number of data-driven elements, that is, to elements represented solely by measurement data. Furthermore, in the considered cases, each nearest neighbor problem is of dimension 2 and the available measurement data set is of cardinality N. Utilizing line search, also referred to as the brute-force approach,

TABLE 1 Computational time needed to solve the nonlinear RC-circuit. Both methods use the trapezoidal rule with a time stepping width of $h = 0.2$. The results show the time for the first 100 time steps.

	Computation time in s			
Method	$N = 10^2$	$N = 10^3$	$N = 10^4$	$N = 10^5$
Data-driven	3.6	5.0	20.9	29.9
Conventional	1.8			

the computational demand of all nearest neighbor problems amounts to $\mathcal{O}(2N_{\mathrm{dd-elem}}N) = \mathcal{O}(N_{\mathrm{dd-elem}}N)$. These costs can be reduced by considering space partitioning techniques, for example, k-d trees, where the query's complexity reduces to $\mathcal{O}(N_{\mathrm{dd-elem}} \log N)$.[33] Note that for small data sets, the brute-force approach is superior, since the space partitioning techniques require training time. Furthermore, adaptively adjusted weighting factors do not comply well with space partitioning techniques, as a retraining would be necessary. Further research in the field of data-driven computing suggested approximate nearest neighbor algorithms in combination with efficient data structures to accelerate the search algorithm.[34] Furthermore, an approach based on hierarchical multi-level data sets has been proposed.[35] As the focus of this work is to showcase that the original data-driven computing framework[8] adapts to ODEs, respectively DAEs, we utilize the line search approach for the nearest neighbor problem, however, with adaptively adjusted weighting factors.

The number of data-driven iterations is strongly connected to the number of employed measurement data. Furthermore, strongly nonlinear element responses demand for more data-driven iterations. In the case of the linear RC-circuit, the number of data-driven iterations per time step vary from 5 (for $N = 10^2$) to 45 (for $N = 10^6$). For the nonlinear RC-circuit, the number of iterations depends on the current operation point in the $(u_{\mathrm{C}}, q_{\mathrm{C}})$ phase-space. In the region where the relation is almost linear, the number of data-driven iterations is similar to the one of the linear RC-circuits. If the operation point is in a strongly nonlinear region, the iterations range from 20 (for $N = 10^2$) to 140 (for $N = 10^6$). In comparison, the traditional solver must solve the nonlinear problem at each time step, which resulted in 12 iterations on average in the case of the nonlinear RC-circuit. Note that the required number of iterations varies depending on the specific problem at hand. The reported values give only a rough estimate of the order of magnitude. A comparison of the data-driven solver and the conventional solver in terms of measured computational time is given in Table 1. The results show the aggregated computational time over the first 100 time steps for the nonlinear RC-circuit, when employing the trapezoidal rule. The results clearly show that the conventional approach is superior against the data-driven approach. Furthermore, the computational time for the data-driven approach increases heavily as larger data sets are employed. However, we emphasize that the most naive approach has been used to solve the nearest neighbor problem and consequently many improvements can be implemented in future works. Considering only a few elements and measurement sets of moderate size, the computational costs of the nearest neighbor Problem (17) can be neglected. However, as more elements are taken into account or as the measurement set becomes larger, the nearest neighbor problem becomes the dominant factor.

Overall, the data-driven MNA solver in its current implementation still needs up to ten times more simulation time. This is the price to pay for the benefit of not requiring models for the circuit elements. It is expected that progress in data-processing will further decrease the gap between traditional and data-driven MNA solvers. Last, we note that the aforementioned remarks on the computational cost of the traditional and the data-driven MNA solvers only take into account the aspect of computational complexity in terms of linear system size, system solutions, and solver iterations. That is, this discussion does not include the effort that is usually needed to identify and construct model representations to be used within traditional MNA solvers. While this element modeling effort is difficult to assess, it must be underlined that the modeling step is bypassed altogether when the data-driven solver is employed.

5 | CONCLUSION

This article developed a data-driven MNA solver which combines Kirchhoff's laws with measurement data for the elements instead of traditional element models. The solver was first applied to a linear RC-circuit, where an investigation on the different approximation errors concluded that the available measurement data and the time stepping size employed in the time integration method should match one another in order to avoid unnecessary computational costs.

The solver was additionally applied to a nonlinear RC-circuit with a voltage-dependent capacitor and to a half-wave rectifier with a data-driven diode. In the former case, the solver achieves a linear convergence rate with respect to the number of measurement data points. This convergence rate is not observed in the latter case, where the switching behavior of the diode model, in particular the regime before the threshold voltage, hinders solver convergence and demands for comparatively large data sets.

The numerical results have shown that the data-driven MNA solver is capable of solving basic circuit problems. Yet, this work acts only as a proof of concept. Several open questions need to be addressed on future research, before a reliable EDA tool can be deployed. These questions include the handling of elements with switching behavior, such as the considered diode, noisy measurement data, temperature dependency, sensitivity and yield analysis, statistical variation for design validation, and the handling of multi-terminal elements, to name but a few. Several problems have already been addressed in the data-driven computing framework for PDEs,[9,34,36] and need to be adapted to circuit problems. However, despite the currently still unresolved challenges, the data-driven and model-free approach remains highly promising, primarily owing to its capacity to mitigate modeling errors and uncertainties while expediting the simulation process for novel components lacking appropriate models.

ACKNOWLEDGMENT

Open Access funding enabled and organized by Projekt DEAL.

FUNDING INFORMATION

This research was supported by the German Research Foundation (DFG) via grants GRK 2128 (project number: 264883531).

CONFLICT OF INTEREST STATEMENT

The authors declare no conflicts of interest.

DATA AVAILABILITY STATEMENT

The data that support the findings of this study are available from the corresponding author upon reasonable request.

ORCID

Armin Galetzka https://orcid.org/0000-0003-3444-8471
Dimitrios Loukrezis https://orcid.org/0000-0003-1264-1182
Herbert De Gersem https://orcid.org/0000-0003-2709-2518

REFERENCES

1. Kurz S, De Gersem H, Galetzka A, et al. Hybrid modeling: towards the next level of scientific computing in engineering. *J Math Ind*. 2022;12(1):8. doi:10.1186/s13362-022-00123-0
2. Wit E, van den Heuvel E, Romeijn JW. 'All models are wrong...': an introduction to model uncertainty. *Stat Neer*. 2012;66(3):217-236.
3. Shockley W. The theory of p-n junctions in semiconductors and p-n junction transistors. *Bell Syst Tech J*. 1949;28(3):435-489. doi:10.1002/j.1538-7305.1949.tb03645.x
4. Kriplani NM, Bowyer S, Huckaby J, Steer MB. Modelling of an Esaki tunnel diode in a circuit simulator. *Act Passive Electron Compon*. 2011;2011:1-8. doi:10.1155/2011/830182
5. Kabir H, Zhang L, Yu M, Aaen PH, Wood J, Zhang QJ. Smart modeling of microwave devices. *IEEE Microw Mag*. 2010;11(3):105-118. doi:10.1109/MMM.2010.936079
6. Ćirić T, Dhuri R, Marinković Z, Pronić-Rančić O, Marković V, Vietzorreck L. Neural based lumped element model of capacitive RF MEMS switches. *Frequenz*. 2018;72(11–12):539-546.
7. Klein DK, Ortigosa R, Martínez-Frutos J, Weeger O. Finite electro-elasticity with physics-augmented neural networks. *Comput Methods Appl Mech Eng*. 2022;400:115501. doi:10.1016/j.cma.2022.115501
8. Kirchdoerfer T, Ortiz M. Data-driven computational mechanics. *Comput Methods Appl Mech Eng*. 2016;304:81-101. doi:10.1016/j.cma.2016.02.001
9. Kirchdoerfer T, Ortiz M. Data driven computing with noisy material data sets. *Comput Methods Appl Mech Eng*. 2017;326:622-641. doi:10.1016/j.cma.2017.07.039
10. Carrara P, De Lorenzis L, Stainier L, Ortiz M. Data-driven fracture mechanics. *Comput Methods Appl Mech Eng*. 2020;372:113390. doi:10.1016/j.cma.2020.113390
11. Kirchdoerfer T, Ortiz M. Data-driven computing in dynamics. *Int J Numer Methods Eng*. 2018;113(11):1697-1710.

12. Bai X, Yang J, Yan W, Huang Q, Belouettar S, Hu H. A data-driven approach for instability analysis of thin composite structures. *Comput Struct*. 2022;273:106898. doi:10.1016/j.compstruc.2022.106898
13. Gerbaud PW, Néron D, Ladevèze P. Data-driven elasto-(visco)-plasticity involving hidden state variables. *Comput Methods Appl Mech Eng*. 2022;402:115394. doi:10.1016/j.cma.2022.115394
14. Ciftci K, Hackl K. Model-free data-driven inelasticity in Haigh-Westergaard space—a study how to obtain data points from measurements. *PAMM*. 2023;22(1):e202200091. doi:10.1002/pamm.202200091
15. De Gersem H, Galetzka A, Ion GI, Loukrezis D, Römer U. Magnetic field simulation with data-driven material modeling. *IEEE Trans Magn*. 2020;56(8):1-6. doi:10.1109/TMAG.2020.3002092
16. Galetzka A, Loukrezis D, De Gersem H. Data-driven solvers for strongly nonlinear material response. *Int J Numer Methods Eng*. 2021;122(6):1538-1562. doi:10.1002/nme.6589
17. Galetzka A, Loukrezis D, De Gersem H. Three-dimensional data-driven magnetostatic field computation using real-world measurement data. *COMPEL*. 2021;41:615-627. doi:10.1108/COMPEL-06-2021-0219
18. Chen X, Wang GF, Zhou W, Zhang QL, Xu JF. Application of neural networks for integrated circuit modeling. In: Wang J, Yi Z, Zurada JM, Lu BL, Yin H, eds. *Advances in Neural Networks—ISNN 2006. Lecture Notes in Computer Science*. Vol 3973. Springer; 2006:1304-1312.
19. Ho CW, Ruehli A, Brennan P. The modified nodal approach to network analysis. *IEEE Trans Circuits Syst*. 1975;22(6):504-509. doi:10.1109/TCS.1975.1084079
20. Meijer PBL. Fast and smooth highly nonlinear multidimensional table models for device modeling. *IEEE Trans Circuits Syst*. 1990;37(3):335-346.
21. Aadithya K, Kuberry P, Paskaleva B, et al. Data-driven compact models for circuit design and analysis. *PMLR*. 2020;107:555-569.
22. Hammouda HB, Mhiri M, Gafsi Z, Besbes K. Neural-based models of semiconductor devices for SPICE simulator. *Am J Appl Sci*. 2008;5(4):385-391.
23. Taunk K, De S, Verma S, Swetapadma A. A brief review of nearest neighbor algorithm for learning and classification. In: 2019 International Conference on Intelligent Computing and Control Systems (ICCS), Madurai, India, 15-17 May 2019. IEEE; 1255-1260. 2019.
24. Bartel T, Harnisch M, Menzel A, Schweizer B. Aspects of accuracy and uniqueness of solutions in data-driven mechanics. *PAMM*. 2023;22(1):e202200206.
25. Nguyen LTK, Aydin RC, Cyron CJ. Accelerating the distance-minimizing method for data-driven elasticity with adaptive hyperparameters. *Comput Mech*. 2022;70(3):621-638. doi:10.1007/s00466-022-02183-w
26. Kanno Y. Mixed-integer programming formulation of a data-driven solver in computational elasticity. *Optim Lett*. 2019;13:1505-1514.
27. Conti S, Müller S, Ortiz M. Data-driven problems in elasticity. *Arch Ration Mech Anal*. 2018;229(1):79-123.
28. Casper T, Duque D, Schöps S, De Gersem H. Automated netlist generation for 3D electrothermal and electromagnetic field problems. *J Comput Electron*. 2019;18(4):1306-1332.
29. Scheier S, Frei S. Characterization and modeling of ESD-behavior of multi layer ceramic capacitors. In: 2013 International Symposium on Electromagnetic Compatibility, Brugge, Belgium, 02-06 September 2013. IEEE; 1028-1033. 2013.
30. Zeltser I, Ben-Yaakov S. On SPICE simulation of voltage-dependent capacitors. *IEEE Trans Power Electron*. 2018;33(5):3703-3710. doi:10.1109/TPEL.2017.2766025
31. Nenzi P, Vogt H. Ngspice Users Manual Version 23. 2011. https://src.fedoraproject.org/repo/extras/ngspice/ngspice23-manual.pdf/eb0d68eb463a41a0571757a00a5b9f9d/ngspice23-manual.pdf
32. Wattel S, Molinari JF, Ortiz M, Garcia-Suarez J. Mesh d-refinement: a data-based computational framework to account for complex material response. *Mech Mater*. 2023;180:104630.
33. Bentley JL. Multidimensional binary search trees used for associative searching. *Comm ACM*. 1975;18(9):509-517.
34. Eggersmann R, Stainier L, Ortiz M, Reese S. Efficient data structures for model-free data-driven computational mechanics. *Comput Methods Appl Mech Eng*. 2021;382:113855.
35. Korzeniowski TF, Weinberg K. A multi-level method for data-driven finite element computations. *Comput Methods Appl Mech Eng*. 2021;379:379. doi:10.1016/j.cma.2021.113740
36. Prume E, Reese S, Ortiz M. Model-free data-driven inference in computational mechanics. *Comput Methods Appl Mech Eng*. 2023;403:115704.

How to cite this article: Galetzka A, Loukrezis D, De Gersem H. Data-driven model-free modified nodal analysis circuit solver. *Int J Numer Model*. 2024;37(2):e3205. doi:10.1002/jnm.3205